Electronic Supplementary Material (ESI) for Energy & Environmental Science.

Supplementary Information

4 V room-temperature all-solid-state sodium battery enabled by a passivating cathode/hydroborate solid electrolyte interface

Ryo Asakura,[1,2] David Reber,[1,3] Léo Duchêne,[1,2] Seyedhosein Payandeh,[1] Arndt Remhof,[1†] Hans Hagemann[2] and Corsin Battaglia[1]

[1] Materials for Energy Conversion, Empa, Swiss Federal Laboratories for Materials Science and Technology, 8600 Dübendorf, Switzerland

[2] Département de Chimie-Physique, Université de Genève, 1211 Geneva 4, Switzerland

[3] Institut des Matériaux, École Polytechnique Fédérale de Lausanne, 1015 Lausanne, Switzerland

[†] e-mail: arndt.remhof@empa.ch

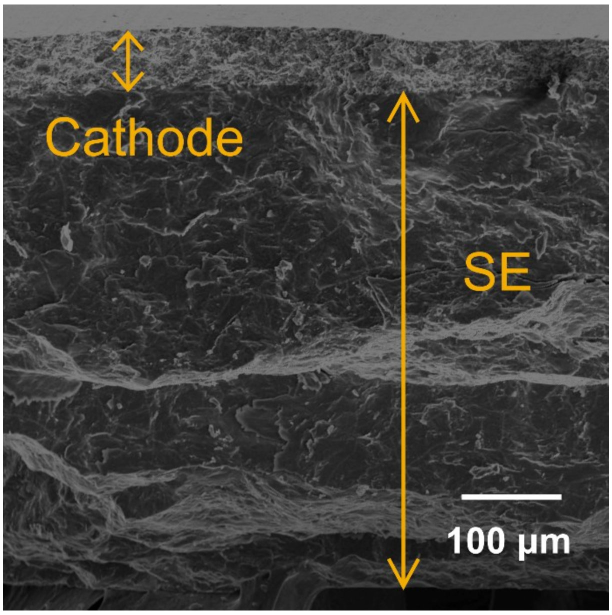

Fig. S1 Full SEM cross-section of the cathode/SE pellet shown in Fig 1.

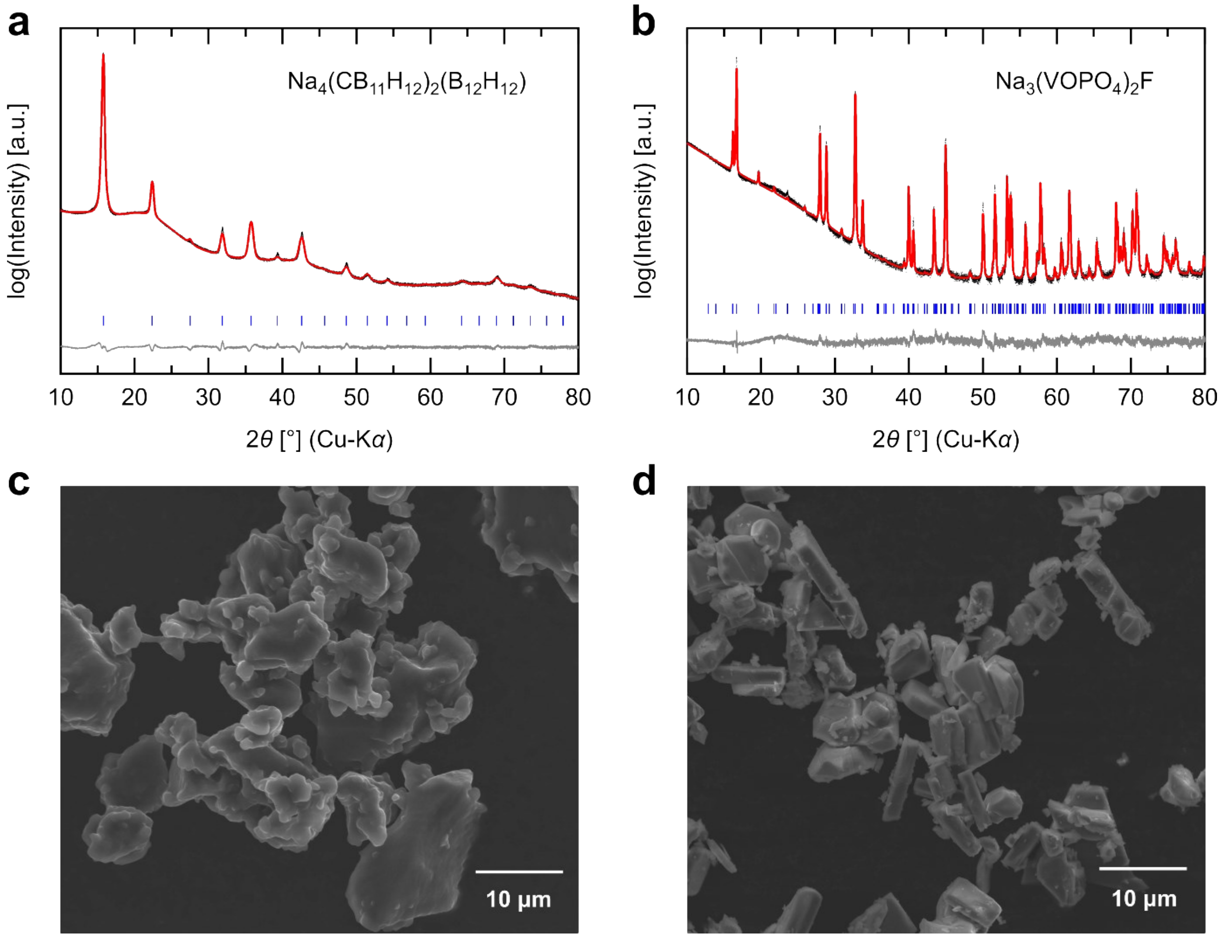

Fig. S2 XRD patterns and Rietveld refinements of as-synthesized (a) $Na_4(CB_{11}H_{12})_2(B_{12}H_{12})$ (R_{wp} = 2.49%, χ^2 = 2.85) and (b) $Na_3(VOPO_4)_2F$ (R_{wp} = 3.66%, χ^2 = 2.00) with the intensity on the log scale. SEM images of as-synthesized (c) $Na_4(CB_{11}H_{12})_2(B_{12}H_{12})$ and (d) $Na_3(VOPO_4)_2F$.

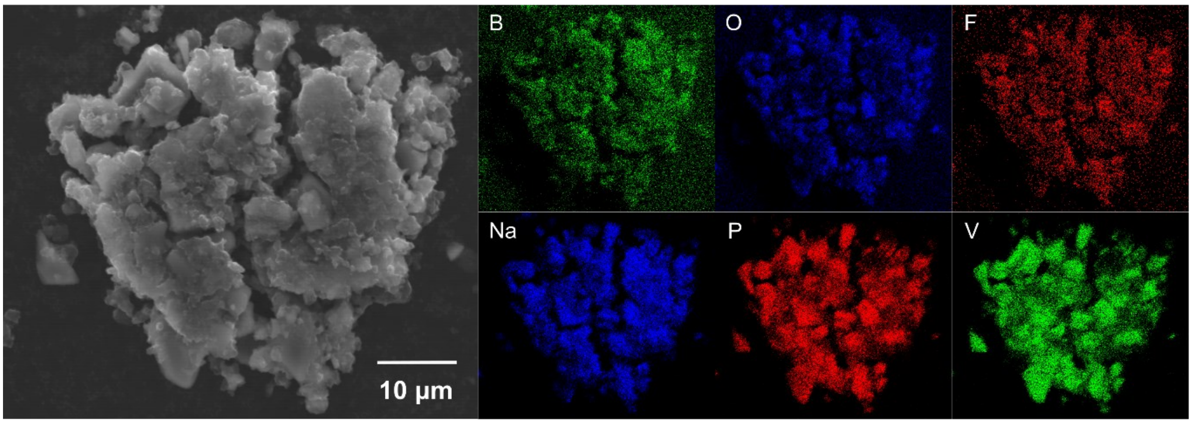

Fig. S3 SEM image and corresponding EDX elemental maps of a cathode composite ($Na_3(VOPO_4)_2F$:$Na_4(CB_{11}H_{12})_2(B_{12}H_{12})$:Carbon = 70:20:10 in weight).

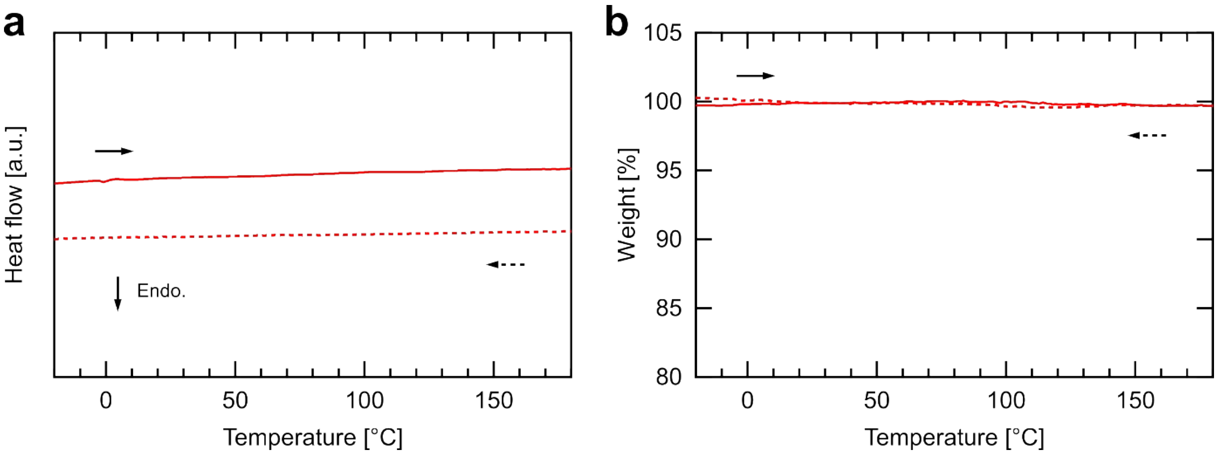

Fig. S4 (a) Differential scanning calorimetry (DSC) and (b) thermogravimetry (TG) data for $Na_4(CB_{11}H_{12})_2(B_{12}H_{12})$ at a heating/cooling rate of 5 °C min^{-1}.

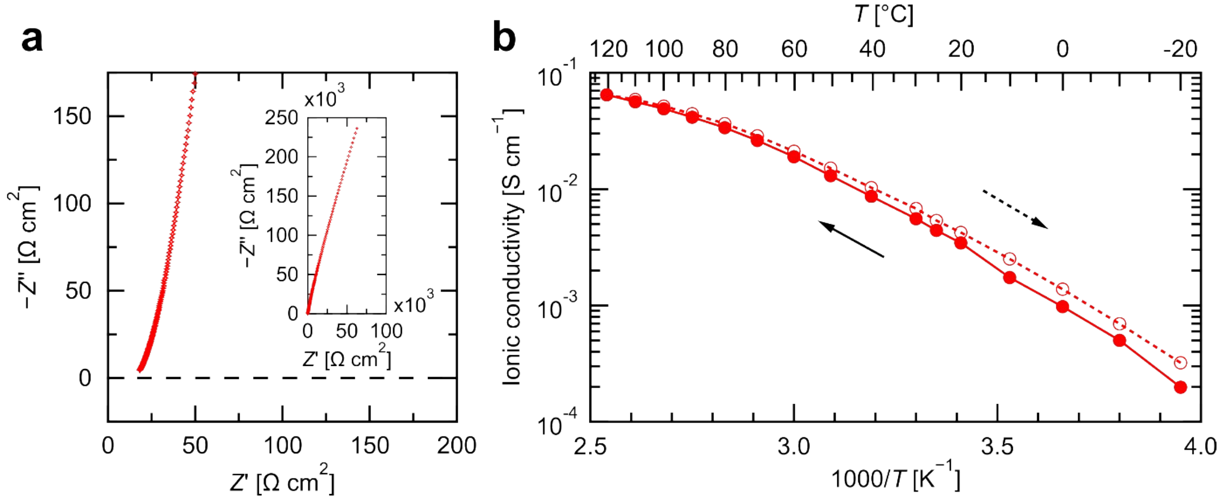

Fig. S5 Ionic conductivity of the $Na_4(CB_{11}H_{12})_2(B_{12}H_{12})$ SE. (a) Nyquist plot at 25 °C and (b) Arrhenius plot of $Na_4(CB_{11}H_{12})_2(B_{12}H_{12})$ between −20 °C and 120 °C during the second heating/cooling. The inset shows the impedance spectra over the full frequency range.

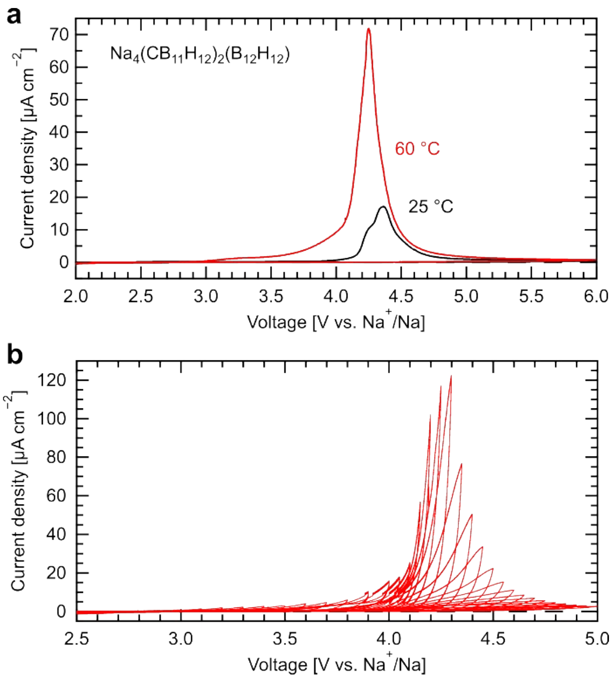

Fig. S6 (a) Cyclic voltammograms of $Na_4(CB_{11}H_{12})_2(B_{12}H_{12})$ in Na/SE/SE-C/Pt cells (SE:Carbon = 75:25 in weight) at a scan rate of 10 μV s^{-1} at 25 °C (black) and at 60 °C (red) (R. Asakura et al., *ACS Appl. Energy Mater.*, 2019, **2**, 6924–6930). (b) Stepwise voltammograms of $Na_4(CB_{11}H_{12})_2(B_{12}H_{12})$ in the same configuration at a scan rate of 50 μV s^{-1} at 60 °C. The upper cutoff voltage was increased by 0.10 V steps from 2.80 V to 4.00 V vs. Na$^+$/Na, followed by 0.05 V steps from 4.00 V to 5.00 V vs. Na$^+$/Na.

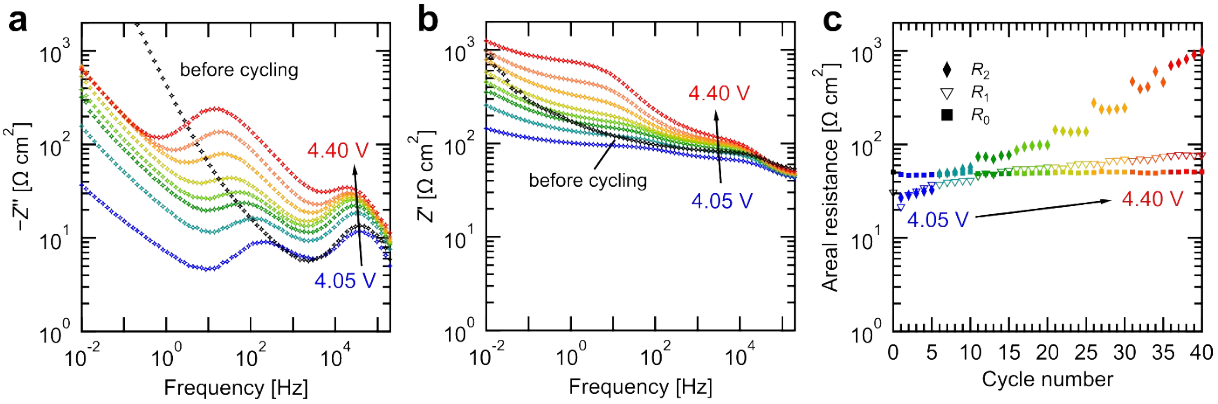

Fig. S7 (a) Imaginary part and (b) real part of the impedance spectra at the initial OCV (denoted as "before cycling") and after a 30 min rest in the second cycle for different upper cutoff voltages during stepwise galvanostatic charge–discharge measurements. (c) Cycle dependence of each resistive contribution of the impedance spectra on a log scale.

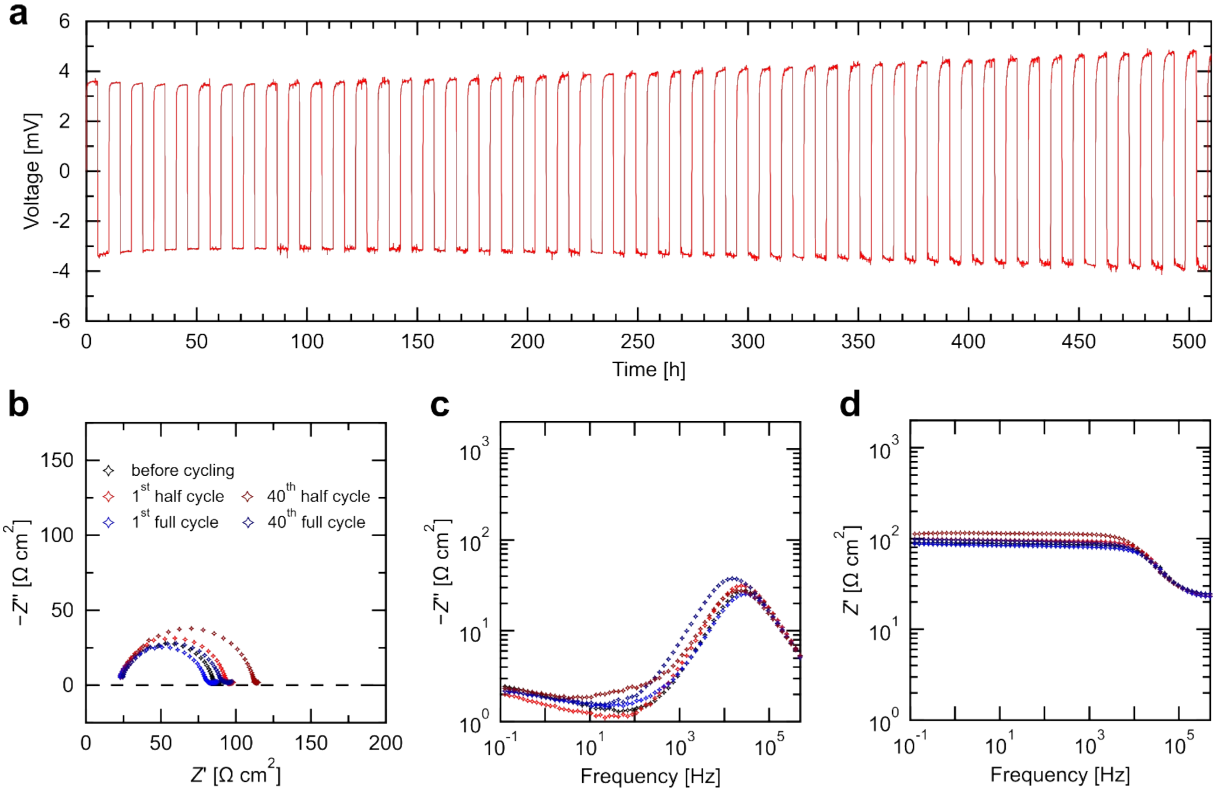

Fig. S8 (a) Galvanostatic cycling of a $Na|Na_4(CB_{11}H_{12})_2(B_{12}H_{12})|Na$ symmetric cell at 25 °C in a Swagelok-type cell (<0.2 MPa) with a current density of 32.2 μA cm^{-2} applied for 5 h, corresponding to 0.161 mAh cm^{-2} per half cycle. (b–d) Nyquist plot and impedance spectra at the initial OCV (denoted as "before cycling") and after a 3 min rest in the first and 40th half and full cycles.

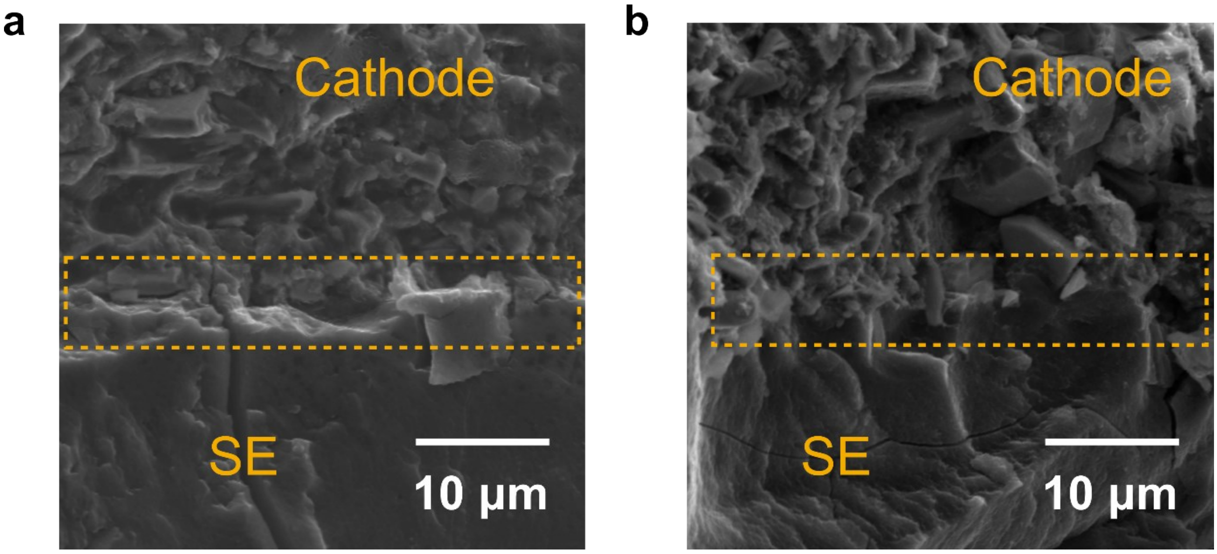

Fig. S9 Cross-sectional SEM images of the cathode/SE interface after long-term cycling between 2.50 V and (a) 4.15 V or (b) 4.30 V vs. Na^+/Na at C/5 following two formation cycles at C/10 at room temperature.

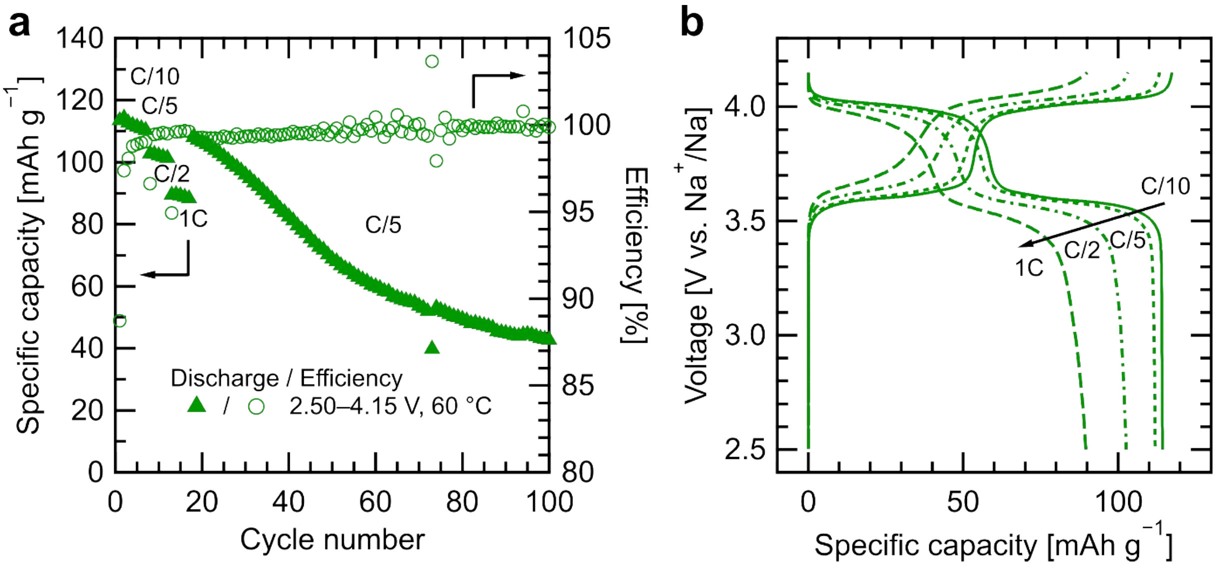

Fig. S10 (a) Rate performance at different C-rates and following cycling performance at C/5 of a $Na_3(VOPO_4)_2F|Na_4(CB_{11}H_{12})_2(B_{12}H_{12})|Na$ all-solid-state cell cycled between 2.50 V and 4.15 V vs. Na^+/Na at 60 °C in a Swagelok-type cell (<0.2 MPa). (b) Corresponding galvanostatic charge–discharge curves in the second cycle at each C-rate.

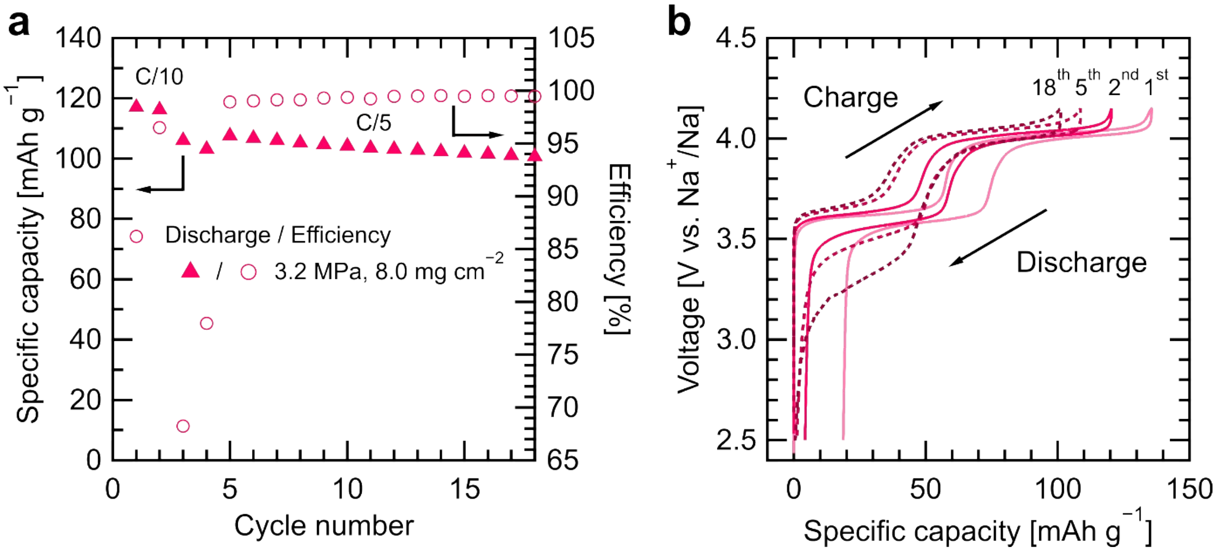

Fig. S11 (a) Cycling performance of a $Na_3(VOPO_4)_2F|Na_4(CB_{11}H_{12})_2(B_{12}H_{12})|Na$ all-solid-state cell cycled between 2.50 V and 4.15 V vs. Na^+/Na at C/5 following two formation cycles at C/10 at room temperature, with a seven-fold mass loading of 8.0 mg cm^{-2} under an external pressure of 3.2 MPa in a pressure cell. (b) Corresponding galvanostatic charge–discharge curves at C/10 (solid) and at C/5 (dashed).

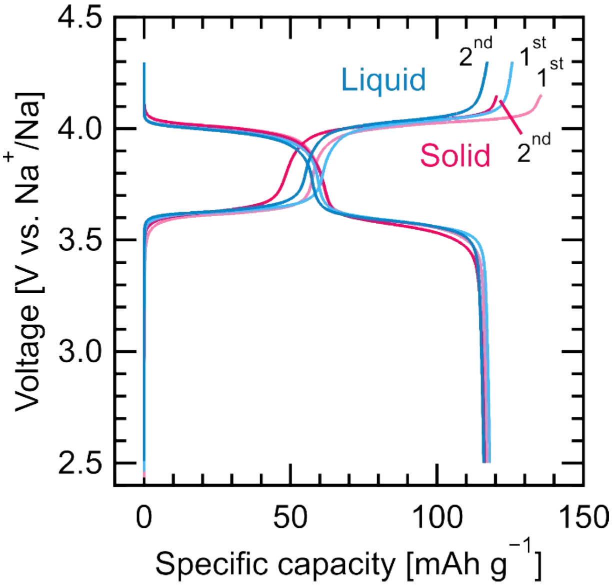

Fig. S12 Comparison of galvanostatic charge–discharge curves of $Na_3(VOPO_4)_2F$ with a sodium metal anode at C/10 in solid (pink) and liquid (blue) electrolytes. The all-solid-state cell shows the same data as in Fig. S11b, while the liquid-electrolyte reference cell was cycled between 2.50 V and 4.30 V vs. Na^+/Na at 25 °C, using 1M $NaClO_4$ in propylene carbonate (PC) : fluoroethylene carbonate (FEC) (98:2 in volume) as a liquid electrolyte.

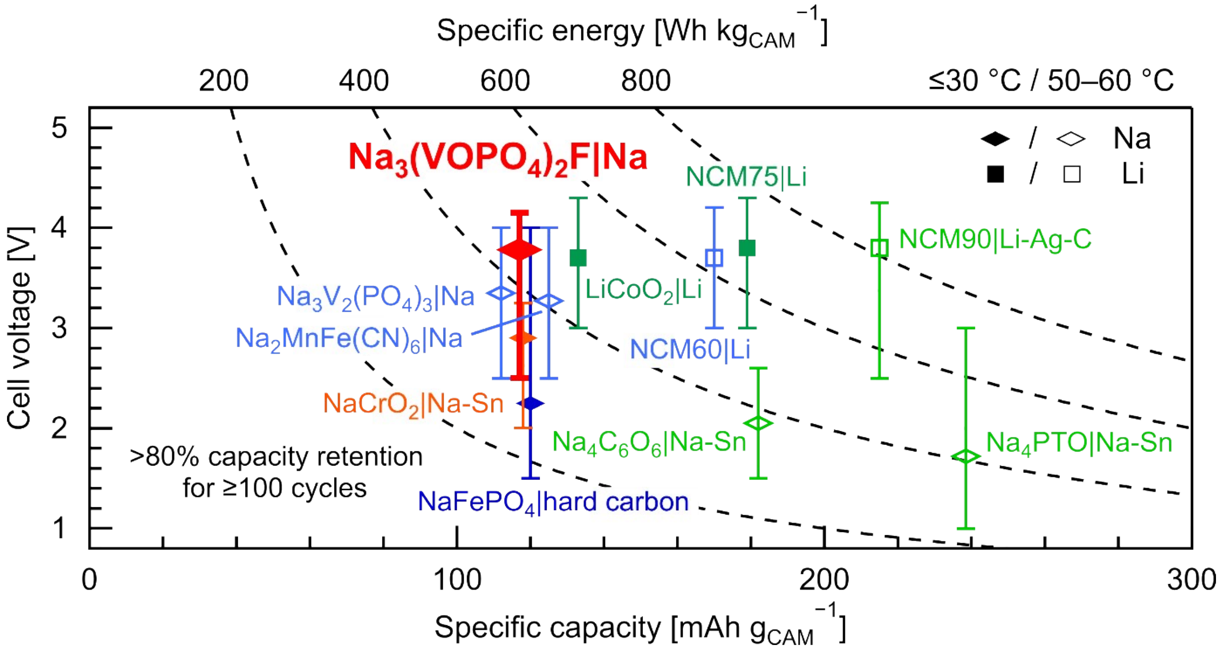

Fig. S13 Comparison of state-of-the-art all-solid-state sodium and lithium battery performance **based on the cathode active material (CAM)**. Specific discharge capacity, average discharge cell voltage, and operating voltage range are plotted for all-solid-state cells exhibiting >80% capacity retention for ≥100 cycles, using in-sertion-type cathode active materials and SEs based on oxides/polymers (blue), sulfides (green), and hydroborates (orange and red). Each specific discharge capacity, **normalized by the cathode active material weight** in sodiated or lithiated states, was measured at C/10, except for NCM60|Li, NCM75|Li, and $NaFePO_4$|hard carbon at C/5, and for Na_4PTO|Na-Sn at C/7.4 (= C/10 for PTO). Cells cycled at room temperature or 30 °C are listed with filled symbols, while empty symbols with a brighter color (sky blue for oxides/polymers and yellow-green for sulfides) refer to long-term cycling at elevated temperatures (50–60 °C). The abbreviations stand for: PTO = pyrene-4,5,9,10-tetraone, NCM90 = $Li[Ni_{0.90}Co_{0.05}Mn_{0.05}]O_2$, NCM75 = $Li[Ni_{0.751}Co_{0.101}Mn_{0.148}]O_2$, and NCM60 = $Li[Ni_{0.60}Co_{0.20}Mn_{0.20}]O_2$.

Table S1 Summary of research targets, achievements in this work, and options for further improvement.

Parameter	Research target	Achieved in this work	Options for further improvement
Cell voltage	>4 V	3.8 V	Higher-voltage cathode with chemical modification of SE & protective coatings
Specific capacity	150 mAh g^{-1}	117 mAh g^{-1} (90% theoretical capacity of 130 mAh g^{-1}) at C/10	Already state-of-the-art sodium-based cathode
Specific energy (per cathode active material (CAM))	600 Wh kg_{CAM}^{-1}	443 Wh kg_{CAM}^{-1}	Already state-of-the-art sodium-based cathode
Cathode composition	>80 wt% active material	70 wt% active material	Optimized particle size and morphology, Reduced carbon & SE content
Specific energy (per cathode composite)	500 Wh $kg_{cathode}^{-1}$	310 Wh $kg_{cathode}^{-1}$	Higher cathode active material composition
Specific energy (per cathode, solid electrolyte (SE), and anode)	400 Wh kg_{cell}^{-1}	33 Wh kg_{cell}^{-1}	Higher mass loading & cathode active material composition, Reduced SE & sodium metal content
Areal capacity	5 mAh cm^{-2}	1 mAh cm^{-2}	Higher mass loading & cathode active material composition
Current density	5 mA cm^{-2}	0.74 mA cm^{-2}	Optimized sodium metal/SE interface
Energy efficiency	>90%	>95%	-
Internal resistance	40 Ω cm^2	85 Ω cm^2	Reduced SE thickness, Optimized sodium metal/SE & cathode/SE interfaces
Cathode composite thickness	Balance between specific energy and current density	50–90 µm	Thicker composite for higher mass loading
Solid electrolyte (SE) thickness	50 µm	500–600 µm	Improved cell assembly process
Cell area	200 cm^2	1.13 cm^2 (Swagelok-type cell), 1.23 cm^2 (Pressure cell)	Pouch-type cell
Pressure	As low as possible	<0.2 MPa (Swagelok-type cell), 3.2 MPa (Pressure cell)	-
Additives	As less binder and carbon as possible	No binder & 10 wt% carbon	Reduced carbon content
Energy retention	80% after 1000 cycles	89% after 400 cycles & 76% after 800 cycles at C/5	-